optica

Monolithic integration of broadband optical isolators for polarization-diverse silicon photonics: supplementary material

YAN ZHANG[1,2†], QINGYANG DU[2†], CHUANGTANG WANG[1†], TAKIAN FAKHRUL[2], SHUYUAN LIU[1], LONGJIANG DENG[1], DUANNI HUANG[3], PAOLO PINTUS[3], JOHN BOWERS[3], CAROLINE A. ROSS[2*], JUEJUN HU[2*], AND LEI BI[1*]

[1] *National Engineering Research Center of Electromagnetic Radiation Control Materials, University of Electronic Science and Technology of China, Chengdu 610054, China*

[2] *Department of Materials Science and Engineering, Massachusetts Institute of Technology, Cambridge, Massachusetts 02139, USA*

[3] *Department of Electrical and Computer Engineering, University of California, Santa Barbara (UCSB), California 93106, USA*

[†] *These authors contributed equally to this work*

**Corresponding authors: caross@mit.edu, hujuejun@mit.edu, bilei@uestc.edu.cn*

Published 12 April 2019

This document provides supplementary information to "Monolithic integration of broadband optical isolators for polarization-diverse silicon photonics," https://doi.org/10.1364/OPTICA.6.000473.

1. STRUCTURAL CHARACTERIZATION OF YIG AND CE:YIG THIN FILMS ON THE ISOLATOR DEVICES

In this section, we present the characterization results for the material structure and composition of Ce:YIG and YIG thin films deposited on the TM and TE isolators on silicon. The chemical composition of YIG and Ce:YIG thin films were measured using inductively coupled plasma mass spectrometry (ICP-MS). Amorphous YIG and Ce:YIG thin films were firstly deposited on SOI substrates at room temperature and then dissolved in nitric acid for ICP-MS characterization. Both materials showed near stoichiometric composition of $Y_{2.91}Fe_{5.00}O_{12}$ and $Ce_{0.99}Y_{2.00}Fe_{5.00}O_{12}$. The crystal structures of YIG/Ce:YIG deposited on SOI were evaluated by standard ω–2θ scans of X-ray diffraction (XRD), as shown in Fig. S1. Both YIG and Ce:YIG layers crystallized into the garnet phase. The lattice constants for YIG and Ce:YIG were 12.37 Å and 12.51 Å, respectively. According to the Scherrer equation, the grain size of YIG and Ce:YIG were calculated to be 36.5 ± 2.7 nm and 34.8 ± 3.1 nm respectively, consistent with TEM analysis. Surface morphology of Ce:YIG was characterized by atomic force microscopy (AFM) both on top of the oxide spacer area and on silicon waveguides, as shown in Fig. S1b. The root mean square (RMS) surface roughness is 5.5 nm on top of oxide spacer and 3.1 nm on top of silicon waveguides for the TM isolator device.

To study the crystallinity and elemental distribution in the garnet film, high resolution TEM images were measured at the MO waveguide cross-sections for both TM and TE isolators. The samples were prepared by focused ion beam milling (FIB). Contact between YIG/Ce:YIG thin films and the waveguide top and sidewalls was observed, as shown in Fig. S1d and S1e. The high resolution TEM image revealed SiO_2 layers of 3-4 nm thickness between YIG and Si, which was formed during the high temperature growth process, and also served as a diffusion barrier between YIG and Si. Well-defined crystal lattices were observed at the YIG side up to the interface. The selected area electron diffraction (SAED) pattern shown in the inset reveals single-phase garnet cubic crystal structures at the device interfaces.

Elemental distributions of Ce, Fe, Y, O and Si were also characterized by energy dispersive spectroscopy (EDS) at the waveguide cross-section for both devices. As an example, Figs. S1 g-k show the results measured on the TE isolator. The Pt layer in Fig. S1 is a protective layer deposited for TEM sample preparation during the focused ion beam milling (FIB) process. This layer filled in the trench between the Si waveguide and YIG/Ce:YIG, indicating a gap between Si and the garnet thin films. Homogeneous elemental distribution and sharp interfaces were observed between the MO materials and Si, indicating high quality magneto-optical thin films growth on the sidewalls of silicon waveguides.

2. PROCESS OPTIMIZATION OF YIG AND CE:YIG THIN FILMS

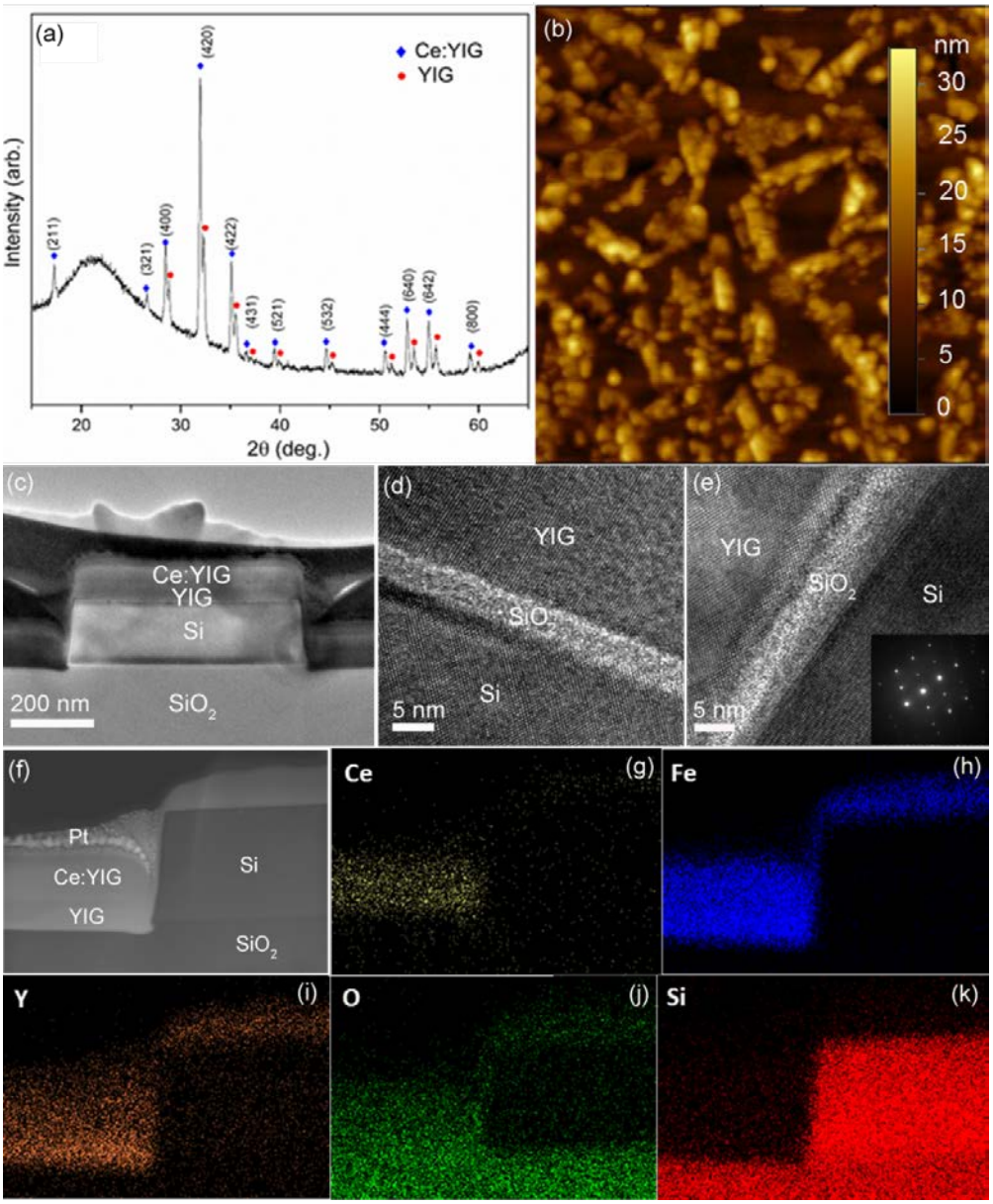

Fig. S1 Crystal structure, morphology and composition of YIG and Ce:YIG thin films deposited on the TM and TE isolators. (a) X-ray diffraction (XRD) pattern of YIG/Ce:YIG thin films grown on a silicon on insulator (SOI). (b) Surface morphology of the YIG/Ce:YIG thin film grown on a SOI substrate measured by atomic force microscopy (AFM). (c) Transmission electron microscopy (TEM) image of the TM isolator and f. TE isolator measured at the MO waveguide cross-sections. (d) High-resolution TEM images of the TM isolator (e) High-resolution TEM of the sidewall (same as TE isolator configuration) at the YIG/Si interface (f), which reveals clear crystal lattice fringes and excellent crystallinity of the garnet materials up to the interface. The inset of (e) also shows the selected area electron diffraction pattern which matches with the garnet cubic crystal structure. (g)-(k) Element distribution at the waveguide cross-section of the TE isolator device show good homogeneity and sharp interfaces of Si, YIG and Ce:YIG materials.

To achieve high Faraday rotation and high magneto-optical figure of merit (FOM) of YIG/Ce:YIG films, we optimized the deposition process of YIG and Ce:YIG thin films. To determine optical loss of YIG seed layer as a function of film thicknesses, 27 nm to 82 nm thick YIG thin films were deposited on 4 μm wide, 220 nm thick SOI waveguides with 3 μm SiO_2 bottom cladding layer to form a magneto-optical waveguide. Propagation loss of the magneto-optical waveguide with different YIG thin films thicknesses were measured using the cut-back method. The confinement factors in YIG and Si were simulated, and then the optical losses of YIG thin films were calculated. The optical loss of YIG monotonically decreases with increasing film thickness, as shown in Fig. S2b. A possible explanation was that the film crystallinity improved with thicker films, therefore leading to lower scattering loss from secondary phases [1]. From the point of view of a high NRPS MO waveguide, the thickness of YIG should be as small as possible. Considering both the device NRPS and material losses, a YIG seed layer thickness of 50 nm was chosen in our experiments.

For Ce:YIG thin film deposition, we mainly controlled the oxygen partial pressure during thin film growth. Based on our first principles calculations, the Ce^{3+} ion population and optical loss of Ce:YIG is strongly dependent on the oxygen vacancy concentrations [2]. To characterize the optical loss, Ce:YIG thin films with a fixed 100 nm thickness were deposited under different oxygen partial pressures on 4 μm wide Si waveguides

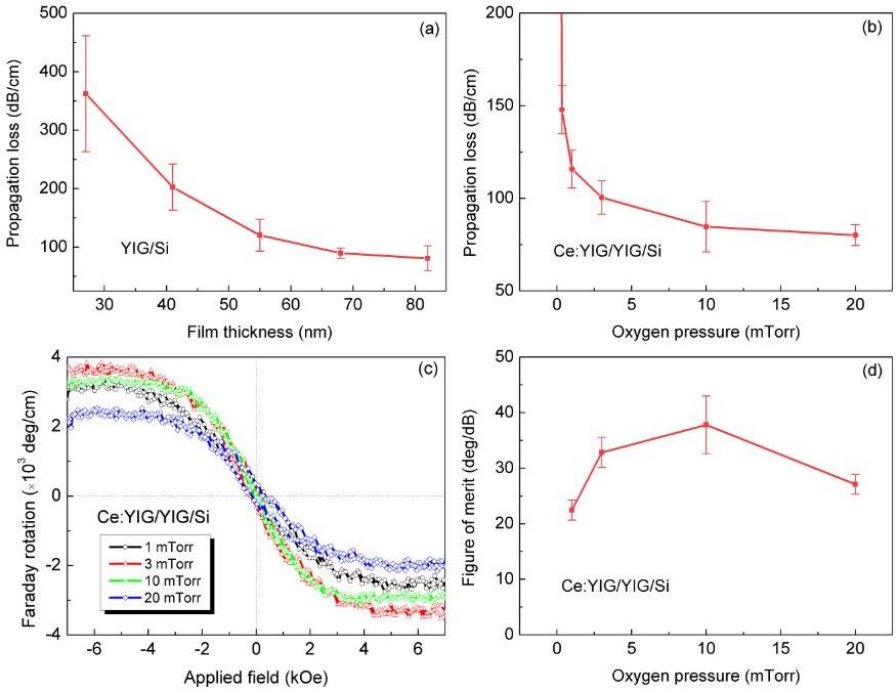

Fig. S2 Optimization of the optical loss and Faraday rotation of YIG and Ce:YIG thin films. (a) Optical loss of YIG thin films as a function of thickness, calculated by MO waveguide propagation losses. (b) Optical loss of Ce:YIG thin films as a function of fabrication oxygen partial pressure measured by MO waveguide propagation losses. (c) The Faraday rotation of Ce:YIG/YIG thin films as a function of Ce:YIG deposition oxygen partial pressure. (d) The figure of merit (FOM) of Ce:YIG thin films as a function of oxygen partial pressure during deposition.

with 50 nm YIG seed layers and the material attenuation was extracted following aforementioned protocols. Fig. S2b plots the Ce:YIG thin film optical loss as a function of the growth oxygen partial pressure. The optical loss of Ce:YIG thin films drastically decreases with increasing oxygen partial pressure during film deposition. A relatively low loss process window is identified at 10 mTorr and above. On the other hand, Faraday rotation of these films is measured using a free-space Faraday rotation characterization setup. The Faraday rotation of these films decreases from -3600 deg/cm, -3000 deg/cm to -2000 deg/cm for growth conditions of 3 mTorr, 10 mTorr and 20 mTorr oxygen partial pressures respectively, due to less Ce^{3+} at high oxygen partial pressures [3]. The trade-off between the optical loss and Faraday rotation of Ce:YIG thin films can be observed by calculating the FOM, *i.e.*, Faraday rotation per length divided by the optical loss per length, as a function of deposition oxygen partial pressures shown in Fig. S2d. The maximum FOM of 38 deg/dB is observed when the deposition oxygen partial pressure is 10 mTorr. This oxygen partial pressure is used in Ce:YIG thin film depositions.

3. ISOLATOR DEVICE CHARACTERIZATION SETUP

The optical isolators were characterized on a fiber butt coupled waveguide test station as shown in Fig. S3. A 1505-1630 nm tunable laser (Keysight 81960A) was firstly fiber coupled to a polarization control bench (Thorlabs, PC-FFB-1550) to generate TE or TM linear polarized light. The linearly polarized light was then coupled to a polarization maintaining fiber and propagated through a 2-by-2 optical switch. The light was butt-coupled into the device through a tapered polarization maintaining fiber, to measure the TE and TM transmittance and finally collected with an optical power sensor (Agilent 81636B). The samples were cleaved at both ends to form end facets. A permanent magnet was placed beside or at the bottom of the sample to introduce an in-plane (~1000 Oe) or out-of-plane (~2500 Oe) magnetic field to saturate the garnet films. The optical switch was used to control the light propagation direction through the devices. All devices were tested at least 3 times by reversing light propagation directions. In the meantime, we also recorded transmission of a straight waveguide on the same chip and with the same width as a reference to acquire device insertion losses. The samples were maintained at room temperature (20 ºC) during the test.

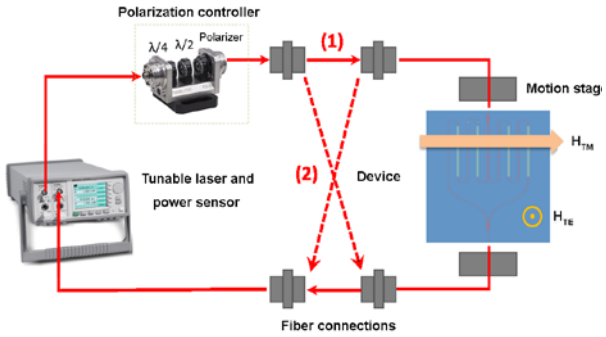

Fig. S3. Schematics of the optical isolator characterization setup. The light propagation direction can be switched forward and backward by switching the fiber connections. The magnetic field direction is also marked for the TM and TE isolators

4. DEVICE PROCESS FLOW

Figure S4 depicts the process flow of the TE and TM isolators on silicon. SOI wafers (Soitec) with 220 nm device layers and 3 µm BOX (buried oxide) layers were used for device fabrication. The wafers were first cleaned in Piranha solutions to remove any organic contaminations. A 4% HSQ resist (XR-1541, Dow Corning) was then spun onto the wafer at 3000 rpm to form a ~100 nm thin resist layer. Device patterns were written by

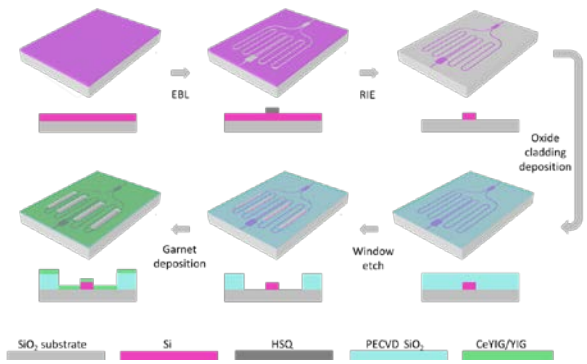

Fig. S4 Process flow of the TE and TM isolators on silicon

electron beam lithography (EBL) at a beam current of 10 nA and an accelerating voltage of 125 kV. The resist was then developed in 25% tetramethylammonium hydroxide (TMAH) for 3 minutes. Subsequently, reactive ion etch (RIE) was utilized to transfer the pattern into the SOI. A layer of FOX-25 (Dow Corning flowable oxide) was then spun onto the wafer at 3000 rpm, followed by rapid thermal annealing (RTA) at 800 ºC for 5 minutes to form the top SiO_2 cladding. To ensure complete isolation of the optical mode from MO material outside the window regions, an additional 200 nm FOX-25 was further spun and annealed. The spin-on glass not only prevents direct contact of MO material with SOI, but also planarizes the wafer to help promote the film growth in subsequent steps. Next, EBL using a positive resist (ZEP520A) was carried out to pattern the window regions. Finally, for TM devices, buffered oxide etch (BOE) was used to expose the silicon waveguide surface. For TE devices, RIE using a CHF_3 and Ar ambient was applied to etch down to the silicon waveguides. A piranha solution was used to clean the samples to remove any fluorinated polymer generated during the etching process. The as-fabricated devices were loaded into the PLD chamber for magneto-optical thin film deposition. 50 nm thick YIG thin films were first deposited onto the substrate at 450 ºC and then rapid thermal annealed (RTA) at 900 ºC for 5 min. Finally, 100 nm thick Ce:YIG thin films were deposited at 650 ºC onto the devices.

5. A MONOLITHIC TE OPTICAL ISOLATOR ON SIN

We also demonstrated a broadband optical isolator based on MZI type SiN devices, as shown in Fig. S5. In this device, we used a fabrication process similar to that used for TE mode SiN ring resonator devices. The SiN TE MZI isolator shows optical isolation ratio of 18 dB and insertion loss around 10 dB, comparable to TE mode Si MZI isolators, further demonstrating this technology is generally applicable to different material platforms and device designs.

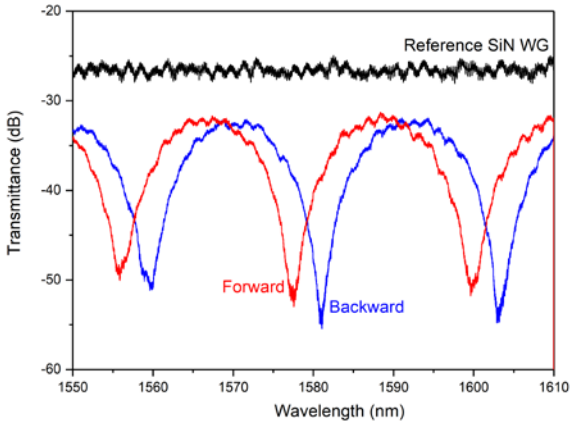

Fig. S5 Forward and Backward transmission spectra of a SiN MZI TE mode optical isolator. Also shown is a single-mode SiN waveguide on the same chip for reference.

6. LOSS ANALYSIS

In this section, we provide a detailed analysis of the device insertion loss. As stated in the manuscript, the insertion loss of our devices is the difference between the loss of the device at forward propagation conditions and the loss of a reference straight waveguide. The insertion loss can be divided into five components as illustrated in Fig. S6. They include: (1) coupler loss; (2) bending loss; (3) junction loss; (4) Si waveguide loss; and (5) MO waveguide loss.

A. TM isolator on Si

The insertion loss of our TM isolator is 5-6 dB, and it can be attributed to different sources as follows,

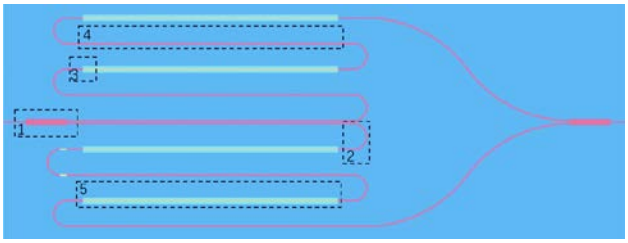

Fig. S6 Loss contributions to the optical isolators on silicon. (1) Coupler loss (2) Bending loss (3) Junction loss (4) Si waveguide loss (5) MO waveguide loss

Table S1 Loss budgets of the TM isolator

Origin of loss	Value(dB)
(1) Coupler loss	1.4
(2) Bending loss	0.001
(3) Junction loss	1
(4) Si WG loss	0.36
(5) MO WG loss	2.2-3.2

(1) *Coupler loss*: The width of the 3 dB MMI coupler input/output port is designed to be 2 μm. From numerical simulations, the loss of each coupler is 0.7 dB. The two couplers lead to 1.4 dB loss. It is possible to reduce this loss by using wider tapered waveguides at the junctions or using adiabatic broadband couplers, see discussions in the manuscript.

(2) *Bending loss*: The curved waveguide bending radius is 20 μm. The bending loss is very small at this radius leading to a total loss of 0.001 dB for all waveguide bends. Due to the large bending radius, the mode field distribution in the curved waveguide is almost the same as that of the straight waveguide. So the loss at the junction between the curved waveguide and the straight waveguide is negligible.

(3) *Junction loss*: At the join between the silicon and MO waveguides, the mode mismatch caused junction loss. The coupling coefficient ω_m can be defined by [4]

$$\omega_m = \frac{\left(\int_{-\infty}^{+\infty}\int_{-\infty}^{+\infty}\vec{z}\cdot(E_S^*\times H_{MO}+E_{MO}\times H_S^*)dxdy\right)^2}{\int_{-\infty}^{+\infty}\int_{-\infty}^{+\infty}\vec{z}\cdot(E_S^*\times H_S+E_S\times H_S^*)dxdy\times\int_{-\infty}^{+\infty}\int_{-\infty}^{+\infty}\vec{z}\cdot(E_{MO}^*\times H_{MO}+E_{MO}\times H_{MO}^*)dxdy}$$

where E_S and H_S represent the mode field in the single-mode waveguide, E_{MO} and H_{MO} represent the mode field of the MO

waveguide. The simulated junction loss is about 0.25 dB per junction, and a total loss of 1 dB results as light passes four times across the junctions in the device.

(4) Si waveguide loss: Compared to the reference straight waveguide, the isolator device has 1.2 mm longer Si waveguides in each arm. The measured propagation loss of the Si waveguide is around 3 dB/cm, leading to excess loss from extra Si waveguides of about 0.36 dB.

(5) *MO waveguide loss*: The rest of the insertion loss is attributed to the magneto-optical waveguide, which is about 2.2-3.2 dB. With the simulated confinement factors shown in Table S2, we can calculate the loss from the MO waveguide of 3.2 dB, in which the silicon waveguide core is estimated to contribute at most 0.2 dB. We assume that the YIG and Ce:YIG layer has the same material loss, leading to a loss value of 50 dB/cm-70 dB/cm for Ce:YIG, in good agreement with the material characterization results shown in Fig. S2b. The Faraday rotation of the Ce:YIG thin films can be evaluated from the measured NRPS value of 19.41 rad/cm, which is -2961 deg/cm. This is also in excellent agreement with the material characterization results. The Ce:YIG material FOM can therefore be fully determined from the device characterization results: 42 deg/dB to 60 deg/dB.

Table S2 Simulated confinement factors in the MO waveguides

Materials and Locations	Confinement Factor
Top YIG	21.4%
Top Ce:YIG	25.0%
Sidewall YIG	2.9%
Sidewall Ce:YIG	2.3%
Si	69.9%

B. TE mode isolators

The loss of the TE mode isolator can also be analyzed similarly. We consider the lowest propagation loss wavelength for the forward propagation light, which is about 4.7 dB from the minimum forward propagation loss in Fig 3b in the manuscript. The loss can be divided into:

Table S3 Loss budgets of the TE isolator

Origin of loss	Value(dB)
(1) Coupler loss	1.5
(2) Bending loss	<0.001
(3) Junction loss	0
(4) Si WG loss	0.44
(5) MO WG loss	2.75

The junction loss is considered 0 thanks to the taper structures. The device shows 9 dB insertion loss as shown in Fig. 3d. The excess 4.3 dB loss is due to the lower NRPS of the MO waveguides compared to simulations. Considering a Faraday rotation of -3000 deg/cm of the Ce:YIG thin film, the simulated NRPS of the MO waveguide is 14 rad/cm. As pointed out in the manuscript, the measured NRPS value of 3.6 rad/cm is lower than this value, possibly due to a lower Faraday rotation of the Ce:YIG thin films for sidewall deposition conditions or air gaps between Si and the MO thin films or an air gap between Ce:YIG and Si.

C. The Si_3N_4 isolator

The loss of the SiN ring resonator can be extracted from its Q quality factor following the analysis protocol we previously established [5]. We measured the transmission spectra of this device before and after MO oxide deposition, yielding a loaded Q factor of ~45,000 and 11,000, respectively, corresponding to a total propagation loss of 4.2 dB/cm and 17.0 dB/cm. The excess 12.8 dB/cm loss comes solely from MO oxide material absorption. Taking account of a modal confinement of 5.4% and again assuming YIG and Ce:YIG are equally lossy, the MO oxide material loss is extracted to be 237 dB/cm. This higher loss compared to Ce:YIG on silicon suggests that further material process optimization is required for SiN devices in the future. In our device design, we have added an adiabatic taper to minimize scatting losses from the window. Therefore, the only junction loss we have is the mode mismatch scattering when light propagates between straight regions and bent regions. The loss is simulated by FIMMPROP software and estimated to be 0.6 dB/cm. As we have a large bending radius of 150 μm, bending loss is <0.01 dB/cm and can be neglected. Our device featured an insertion loss of 11.5 dB. The loss contributions are summarized in Table S4. Meanwhile, we extrapolate the NRPS of MO oxide film from the peak shift and estimated to be ~ -1400 degree/cm.

Table S4 Loss budgets of the SiN TE isolator

Origin of loss	Value(dB)
(1) Bending loss	<0.01
(2) Junction loss	0.4
(3) SiN WG loss	2.4
(4) MO WG loss	7.7

7. RETICLE DESIGNS: DEVICE LAYOUT

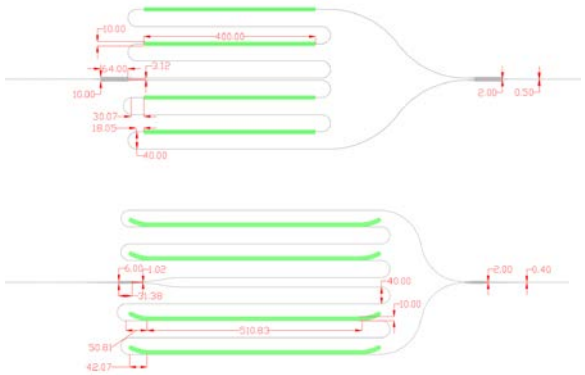

Fig. S7 Device design layout of the TE and TM isolators on silicon. The lengths are in micrometers.

REFERENCES

1. 1. A. D. Block, P. Dulal, B. J. H. Stadler and N. C. A Seaton, "Growth Parameters of Fully Crystallized YIG, Bi:YIG, and Ce:YIG films with High Faraday Rotations," IEEE Photonics J., **6**, 600308 (2014).
2. X. Liang, J. Xie, L. Deng and L. Bi, "First principles calculation on the magnetic, optical properties and oxygen vacancy effect of $Ce_xY_{3-x}Fe_5O_{12}$," *Appl. Phys. Lett.*, **106**, 052401 (2015) .
3. Y. Zhang, C. Wang, X. Liang, B. Peng, H. Lu, P. Zhou, L. Zhang, J. Xie, L. Deng, M. Zahradnik, L. Beran, M. Kucera, M. Veis, C. A. Ross and L. Bi, "Enhanced magneto-optical effect in $Y_{1.5}Ce_{1.5}Fe_5O_{12}$ thin films deposited on silicon by pulsed laser deposition," J. Alloy Compd., **703**, 591-599 (2017).

4. M. Lohmeyer and R. Stoffer, “Integrated optical cross strip polarizer concept,” Opt. Quant. Electron, **33**, 413-431 (2001).
5. L. Bi, J. Hu, P. Jiang, D. H. Kim, G. F. Dionne, L. C. Kimerling and C. A. Ross, “On-chip optical isolation in monolithically integrated non-reciprocal optical resonators,” Nat. Photonics **5**, 758–762 (2011).